The Astrophysical Journal Letters, 898:L11 (6pp), 2020 July 20 https://doi.org/10.3847/2041-8213/ab9eb9

NGTS-11 b (TOI-1847 b): A Transiting Warm Saturn Recovered from a TESS Single-transit Event

Samuel Gill[1,2], Peter J. Wheatley[1,2], Benjamin F. Cooke[2], Andrés Jordán[3,4], Louise D. Nielsen[5], Daniel Bayliss[2], David R. Anderson[2], Jose I. Vines[6], Monika Lendl[5,7], Jack S. Acton[8], David J. Armstrong[1,2], François Bouchy[5], Rafael Brahm[3,4], Edward M. Bryant[1,2], Matthew R. Burleigh[8], Sarah L. Casewell[8], Philipp Eigmüller[9], Néstor Espinoza[10], Edward Gillen[11,20], Michael R. Goad[8], Nolan Grieves[5], Maximilian N. Günther[12,21], Thomas Henning[13], Melissa J. Hobson[4,14], Aleisha Hogan[8], James S. Jenkins[6,15], James McCormac[2], Maximiliano Moyano[16], Hugh P. Osborn[12,17], Don Pollacco[1,2], Didier Queloz[11], Heike Rauer[9], Liam Raynard[8], Felipe Rojas[4,14], Paula Sarkis[13], Alexis M. S. Smith[9], Marcelo Tala Pinto[4,18], Rosanna H. Tilbrook[8], Stéphane Udry[5], Christopher A. Watson[19], and Richard G. West[2]

[1] Centre for Exoplanets and Habitability, University of Warwick, Gibbet Hill Road, Coventry CV4 7AL, UK; samuel.gill@warwick.ac.uk
[2] Department of Physics, University of Warwick, Gibbet Hill Road, Coventry CV4 7AL, UK
[3] Facultad de Ingeniería y Ciencias, Universidad Adolfo Ibáñez, Av. Diagonal las Torres 2640, Peñalolén, Santiago, Chile
[4] Millennium Institute for Astrophysics, Chile
[5] Observatoire astronomique de l'Université de Genève, Chemin des maillettes 51, 1290 Sauverny, Switzerland
[6] Departamento de Astronomía, Universidad de Chile, Camino El Observatorio 1515, Las Condes, Santiago, Chile
[7] Space Research Institute, Austrian Academy of Sciences, Schmiedlstr. 6, A-8042 Graz, Austria
[8] School of Physics and Astronomy, University of Leicester, University Road, Leicester LE1 7RH, UK
[9] Institute of Planetary Research, German Aerospace Center, Rutherfordstrasse 2, D-12489, Berlin, Germany
[10] Space Telescope Science Institute, 3700 San Martin Drive, Baltimore, MD 21218, USA
[11] Astrophysics Group, Cavendish Laboratory, J.J. Thomson Avenue, Cambridge CB3 0HE, UK
[12] Department of Physics and Kavli Institute for Astrophysics and Space Research, Massachusetts Institute of Technology, 70 Vassar Street, Cambridge, MA 02139, USA
[13] Max-Planck-Institut für Astronomie, Königstuhl 17, D-69117 Heidelberg, Germany
[14] Instituto de Astrofísica, Facultad de Física, Pontificia Universidad Católica de Chile, Chile
[15] Centro de Astrofísica y Tecnologías Afines (CATA), Casilla 36-D, Santiago, Chile
[16] Instituto de Astronomía, Universidad Católica del Norte, Angamos 0610, 1270709 Antofagasta, Chile
[17] NCCR/PlanetS, Centre for Space & Habitability, University of Bern, Bern, Switzerland
[18] Landessternwarte, Zentrum für Astronomie der Universität Heidelberg, Königstuhl 12, D-69117 Heidelberg, Germany
[19] Astrophysics Research Centre, School of Mathematics and Physics, Queen's University Belfast, Belfast BT7 1NN, UK
Received 2020 April 30; revised 2020 June 13; accepted 2020 June 16; published 2020 July 20

Abstract

We report the discovery of NGTS-11 b (=TOI-1847b), a transiting Saturn in a 35.46 day orbit around a mid K-type star ($T_{\rm eff} = 5050 \pm 80$ K). We initially identified the system from a single-transit event in a TESS full-frame image light curve. Following 79 nights of photometric monitoring with an NGTS telescope, we observed a second full transit of NGTS-11 b approximately one year after the TESS single-transit event. The NGTS transit confirmed the parameters of the transit signal and restricted the orbital period to a set of 13 discrete periods. We combined our transit detections with precise radial-velocity measurements to determine the true orbital period and measure the mass of the planet. We find NGTS-11 b has a radius of $0.817\pm^{0.028}_{0.032}\,R_{\rm Jup}$, a mass of $0.344\pm^{0.092}_{0.073}\,M_{\rm Jup}$, and an equilibrium temperature of just $435\pm^{34}_{32}$ K, making it one of the coolest known transiting gas giants. NGTS-11 b is the first exoplanet to be discovered after being initially identified as a TESS single-transit event, and its discovery highlights the power of intense photometric monitoring in recovering longer-period transiting exoplanets from single-transit events.

Unified Astronomy Thesaurus concepts: Exoplanet astronomy (486); Exoplanet detection methods (489); Exoplanets (498); Extrasolar gas giants (509); Photometry (1234); High resolution spectroscopy (2096)

Supporting material: data behind figure

1. Introduction

Wide-field photometric surveys have uncovered a large population of transiting exoplanets around bright stars (e.g., Bakos et al. 2004; Pollacco et al. 2006; Borucki et al. 2010), providing key opportunities to measure precise planetary radii and densities, constrain bulk composition, and to characterize planetary atmospheres (e.g., Seager & Mallén-Ornelas 2003; Fortney et al. 2007; Sing et al. 2016). However, the transit geometry imposes a strong selection bias for close-in orbits, and only a handful of well-characterized transiting exoplanets are known to have orbital periods longer than about 30 days. This limits our characterization of the wider exoplanet population, as well as its evolution through planetary migration (e.g., Jones et al. 2004; Nottale et al. 2004; Alibert et al. 2013). It also prevents us from using transits to characterize exoplanets in the habitable zone (Kasting et al. 1993;

[20] Winton Fellow.
[21] Juan Carlos Torres Fellow.

Kopparapu et al. 2013), except around very late-type host stars (e.g., Gillon et al. 2017).

The extremely wide field of the TESS survey (Ricker et al. 2015) is providing many new exoplanet candidates around bright stars. Longer-period planets can be confirmed at high ecliptic latitudes, where TESS monitors stars for up to one year (e.g., Dalba et al. 2020; Eisner et al. 2020). However, with an observing baseline of only 27 days across most of the sky, TESS typically detects only a single transit for longer-period planets (Cooke et al. 2018; Villanueva et al. 2019). Follow-up of these single-transit events provide the opportunity to discover and characterize many more longer-period planets (Yee & Gaudi 2008; Yao et al. 2019). However, a single-transit event provides only a weak constraint on the orbital period of the planet (Osborn et al. 2016; Sandford et al. 2019), so follow-up observations designed to confirm the exoplanet are expensive, whether aiming to detect additional transits, or to detect the radial-velocity variations of the host star.

The NGTS project (Wheatley et al. 2018) has commenced a program to follow-up TESS single-transit event candidates, and has already discovered three longer-period, low-mass eclipsing binary systems: TIC-238855958 (Gill et al. 2020a), TOI-222 (Lendl et al. 2020), and TIC-231005575 (Gill et al. 2020b).

In this Letter we present the first discovery of an exoplanet based on a single-transit event from TESS. We show how an observing strategy focusing on detecting a second transit, in this case with NGTS, enables longer-period planets to be confirmed and characterized using a very modest number of radial-velocity measurements.

2. Observations and Analysis

2.1. TESS Single-transit Detection

Using light curves produced from the TESS calibrated full-frame images by Oelkers & Stassun (2018), we conducted a systematic search for single-transit events using the procedure described by Gill et al. (2020a).

The K-dwarf TIC-54002556 (hereafter NGTS-11, $T = 11.62$, properties in Table 1) was observed at a 30 minute cadence with TESS Camera 1 in Sector 3 of the mission (2018 September 20–2018 October 18). NGTS-11 was not selected for TESS 2 minute cadence observations, so it does not have a light curve from the SPOC pipeline.

We identified a promising single-transit event from NGTS-11 approximately 9 days into Sector 3, at JD 2458390.7, with a transit width of 4 h and depth of 1% (shown in the top panel of Figure 1). We inspected the individual TESS calibrated full-frame images for asteroids and any other anomalies. We also searched for blended objects in Gaia DR2 (Gaia Collaboration et al. 2018) and checked for known nearby exoplanets or eclipsing binaries that might be the source of the transit event. We found no reason to believe this single-transit candidate was a false positive.

Having identified NGTS-11 as hosting a viable exoplanet candidate, we created a higher-quality TESS light curve from the TESS calibrated full-frame images by carefully selecting source and background pixel apertures in order to minimize blending with neighboring objects. Background pixels were selected from a 15 × 15 pixel median master frame using an iterative sigma-clipping process. Source pixels were selected from a central 7 × 7 pixel region where median pixel counts exceeded the background level by 100 times the standard deviation in the background. To exclude source pixels contaminated by neighboring objects, we also required a monotonic decrease in counts with distance from the target position. The final source aperture included 19 pixels.

These apertures better exclude fainter, nearby companions TIC-54002560 (48.″51; $T = 14.28$) and TIC-54002559 (56.″41; $T = 14.51$). Frames with a quality flag larger than 0 were rejected, and the light curve was detrended using a median filter of width 10.5 hr. The resulting TESS light curve around the time of the transit is shown in Figure 1, and this was used for the remainder of this work.

Table 1
Cataloged, Measured, and Derived Properties of NGTS-11 and NGTS-11 b

Catalog Data		Model Parameters	
TIC ID	TIC-54002556	T_0 (BJD-TDB)	2458390.7043 ± 0.0016
R.A.	$01^h34'05.''15$	P (d)	35.45533 ± 0.00019
Decl.	$-14°25'08.''9$	$R_\star/a$	$0.0183\pm^{0.0029}_{0.0025}$
G	12.1895 ± 0.0002	$R_p/R_\star$	$0.1010\pm^{0.0030}_{0.0037}$
BP	12.6725 ± 0.0012	b	$0.81\pm^{0.13}_{0.10}$
RP	11.5707 ± 0.0011	$h_{1,\mathrm{TESS}}$	$0.7406\pm^{0.0030}_{0.0030}$
pmRA (mas yr^{-1})	11.168 ± 0.099	$h_{2,\mathrm{TESS}}$	$0.427\pm^{0.046}_{0.046}$
pmDec (mas yr^{-1})	14.047 ± 0.049	$h_{1,\mathrm{NGTS}}$	$0.7144\pm^{0.0031}_{0.0030}$
Parallax (mas)	5.223 ± 0.048	$h_{2,\mathrm{NGTS}}$	$0.442\pm^{0.043}_{0.046}$
TESS(T)	11.624 ± 0.006	$l_{3,\mathrm{TESS}}$	$0.051\pm^{0.048}_{0.034}$
APASS9 (B)	13.308 ± 0.035	$K_\star$ (km s^{-1})	$0.0212\pm^{0.0046}_{0.0041}$
APASS9(V)	12.456 ± 0.080	$\sqrt{e}\sin\omega$	$0.13\pm^{0.26}_{0.28}$
APASS9 (g')	12.852 ± 0.038	$\sqrt{e}\cos\omega$	$0.19\pm^{0.16}_{0.22}$
APASS9 (r')	12.127 ± 0.012	γ (km s^{-1})	$21.4094\pm^{0.0029}_{0.0028}$
APASS9 (i')	11.864 ± 0.083	$\Delta\gamma_{\mathrm{FEROS}}$ (km s^{-1})	$-0.042\pm^{0.010}_{0.010}$
2MASS (J)	10.855 ± 0.025	Derived planet properties	
2MASS (H)	10.401 ± 0.023	$M_p(M_{\mathrm{Jup}})$	$0.344\pm^{0.092}_{0.073}$
2MASS (K_s)	10.315 ± 0.025	$R_p(R_{\mathrm{Jup}})$	$0.817\pm^{0.028}_{0.032}$
Stellar parameters		a(au)	$0.2010\pm^{0.0021}_{0.0022}$
T_{eff} (K)	5050 ± 80	e	$0.13\pm^{0.10}_{0.09}$
[Fe/H] (dex)	0.22 ± 0.08	ω (deg)	$32\pm^{53}_{76}$
$\log g_\star$ (dex)	4.5 ± 0.1	i (deg)	$89.16\pm^{0.20}_{0.29}$
$v \sin i$ (km s^{-1})	1.1 ± 0.8	T_{dur} (hr)	$3.59\pm^{0.18}_{0.37}$
$M_\star(M_\odot)$	0.862 ± 0.028	g_p (m s^{-2})	$14.1\pm^{5.3}_{3.4}$
$R_\star(R_\odot)$	0.832 ± 0.013	T_{eq}(K)	$435\pm^{34}_{32}$
$\rho_\star$ ($\rho_\odot$)	1.496 ± 0.085	ρ_p (g cm^{-3})	$0.78\pm^{0.21}_{0.17}$
Age (Gyr)	3.9 ± 1.6	H_p (km)	$141\pm^{74}_{51}$

2.2. A Second Transit with NGTS

We used the NGTS facility (Wheatley et al. 2018) located at the ESO Paranal Observatory in Chile to monitor NGTS-11 photometrically, searching for additional transits. NGTS was designed specifically for very high-precision photometry of exoplanet transits, and it is thus well suited to photometric follow-up of TESS single-transit candidates (Wheatley et al. 2018). We started monitoring NGTS-11 with a single NGTS telescope on the night of 2019 August 11. We observed each subsequent night with 10 s exposures whenever the target was above an elevation of 30 deg and weather conditions allowed. The images were reduced to light curves each day using the

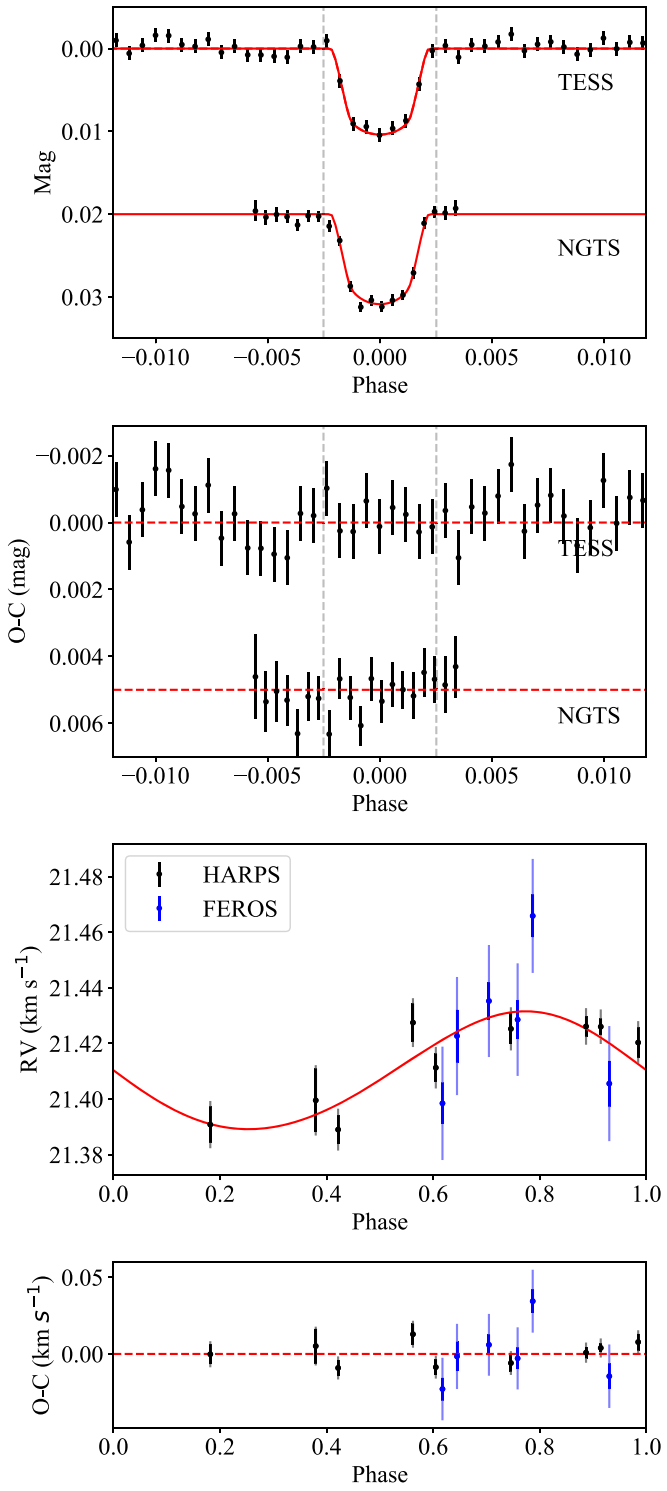

Figure 1. Our best-fitting model to the photometric and radial-velocity observations of NGTS-11. The upper panel shows the transit photometry of TESS and NGTS, with the model in red. Dashed vertical gray lines indicate the start of ingress and end of egress. Photometric residuals are shown in the upper middle panel. NGTS photometry has been binned to 30 minutes for plotting purposes, but was fitted at the full 13 s time resolution. The lower panels show the radial-velocity observations and residuals from FEROS (blue) and HARPS (black), along with our best-fitting model (red). Semi-transparent error bars represent uncertainties with jitter values added in quadrature.

(The data used to create this figure are available.)

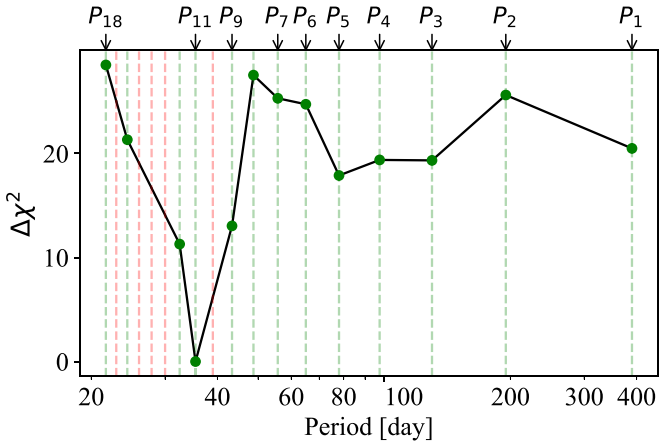

Figure 2. The relative goodness-of-fit for different candidate orbital periods from our joint fits to the TESS and NGTS transit detections and radial-velocity measurements of NGTS-11 (described in Section 2.6). Priors were used to constrain each fit to orbital periods around those allowed by the TESS and NGTS photometry (green dashed lines). Orbital periods excluded by NGTS observations are marked in red (see Section 2.3). Our best fit is to P_{11} (=390.0082/11 = 35.46 days).

on-site NGTS real-time aperture photometry pipeline described by Bryant et al. (2020).

We used the template matching algorithm described by Gill et al. (2020a, 2020b) to search the NGTS light curve for additional transit events. This involved using a model fit to the TESS transit as a template, which was placed at each possible transit epoch within the NGTS light curve and the improvement in log-likelihood calculated ($\Delta \log \mathcal{L} = -\Delta\chi^2/2$). From empirical injection tests, we conservatively estimated that a significant template match would be consistent with $\Delta \log \mathcal{L} > 50$. We observed NGTS-11 for 79 nights (105 642 exposures) before a second transit event was detected ($\Delta \log \mathcal{L} = 364$) on the UT night of 2019 October 24. The transit event was centered at JD 2458780.712, which is 390 days after the initial TESS single-transit. The NGTS transit detection is plotted in the top panel of Figure 1.

2.3. Photometric Constraints on Orbital Period

We measured the precise separation of the TESS and NGTS transit detections using a joint transit fit to both light curves, finding $\Delta T = 390.0082 \pm 0.0032$ days. The orbital period of the companion to NGTS-11 must be an integer fraction of this duration. We label these candidate periods as $P_n = (390.0082/n)$, where n is an integer. These candidate periods are indicated with vertical lines in Figure 2.

All candidate periods beyond P_{18} were ruled out by the TESS data, since additional transits would have been detected. Similarly, five candidate periods (P_{10}, P_{13}, P_{14}, P_{15}, and P_{17}) were ruled out by the NGTS photometric monitoring as well as additional observations on 2019 November 22 and 2019 December 1 (red dashed vertical lines in Figure 2). This left just 13 candidate orbital periods (green dashed vertical lines in Figure 2).

2.4. Radial-velocity Measurements

Following the NGTS transit detection, we immediately began radial-velocity follow-up using the CORALIE fiber-fed

Échelle spectrograph installed on the 1.2 m Leonard Euler telescope at the ESO La Silla Observatory (Queloz et al. 2001). We made three 600 s observations of NGTS-11 over 54 days (2019 October 29, November 28, and December 25), the first just 5 days after the NGTS transit detection. The spectra were reduced using the CORALIE standard reduction pipeline, with radial-velocity measurements derived using the cross-correlation technique and a numerical G2 mask. The radial velocities had no variation above 80 m s^{-1}, showing that the transiting companion is unlikely to be a low-mass star.

This motivated an additional nine 1800 s radial-velocity measurements spanning 63 days with the HARPS spectrograph ($R = 115{,}000$) on the 3.6 m ESO telescope (Pepe et al. 2002), and six measurements spanning 11 days with the FEROS spectrograph ($R = 48{,}000$) on the MPG/ESO 2.2 m Telescope (Kaufer et al. 1999). The FEROS data were reduced with the CERES pipeline (Brahm et al. 2017). These data are plotted in the lower panels of Figure 1.

2.5. Stellar Properties

We used our HARPS spectra to determine the properties of the host star NGTS-11. The individual spectra were shifted to the laboratory frame of reference and coadded to produce a combined spectrum with a signal-to-noise ratio of 44. We used ISPEC (Blanco-Cuaresma et al. 2014) to synthesize models using the the radiative transfer code SPECTRUM (Gray 1999), MARCS model atmospheres (Gustafsson et al. 2008), and version 5 of the GAIA ESO survey (GES) atomic line list within ISPEC with solar abundances from Asplund et al. (2009). We used the Hα, Na I D, and Mg I b lines to determine the stellar effective temperature, $T_{\rm eff}$, and surface gravity, $\log g$. We used individual FeI and FeII lines to determine metallicity, [Fe/H], and the rotational broadening projected into the line of sight, $v \sin i$. Values of macroturbulence and microturbulence were calculated using Equations (5.10) and (3.1), respectively, from Doyle (2015).

We used the method described in Gill et al. (2020a) to determine the mass, radius, and age of NGTS-11. This method uses Gaia magnitudes and parallax (Gaia Collaboration et al. 2018) along with $T_{\rm eff}$ and [Fe/H] from our spectroscopy to determine the best-fitting stellar parameters with respect to MESA models (Choi et al. 2016; Dotter 2016).

The results of our analysis are presented in Table 1. We find that NGTS-11 is a mid K-dwarf star ($T_{\rm eff} = 5050 \pm 80$ K) with a super-solar metallicity of [Fe/H] $= 0.22 \pm 0.08$.

2.6. Orbital Period and Planet Properties

In order to determine the true orbital period of NGTS-11 b, as well as its physical properties, we carried out joint fits of our transit light curves (TESS and NGTS) and radial-velocity data (HARPS and FEROS) at each of the candidate orbital periods allowed by the photometry (see Section 2.3 and Figure 2).

A perfect minimization algorithm would explore the whole parameter space in a single fit, finding each of the thirteen orbital periods allowed by the photometry for itself. However, the χ^2 minima are narrow and widely spaced, and this approach is not efficient in practice. Instead, we explored each minimum with a separate MCMC run, using a uniform prior that selected the period alias in question, but did not define the period itself. Figure 2 shows the best χ^2 from each of these 13 runs, mapping the depth of each χ^2 minimum.

Our model has 17 free parameters, with best-fitting values presented in Table 1, and the best-fitting model shown in Figure 1. In addition to the orbital period, P, these include T_0, the TESS transit epoch, R_*/a, R_p/R_*, and the transit impact parameter, b, where R_* is the radius of the star, R_p is the radius of the planet, and a is the orbital separation. For the TESS and NGTS transit data we also fit for the out-of-transit magnitude offsets, as well as the decorrelated limb-darkening parameters h_1 and h_2 from Maxted (2018). We employed Gaussian priors on h_1 and h_2 for each instrument interpolated from Maxted (2018) using stellar atmospheric parameters from Section 2.5. These priors dominate the posterior distributions for h_1 and h_2. In our initial fits we found that the TESS transit was slightly shallower than the NGTS transit, which we ascribe to residual blending with the neighboring stars mentioned in Section 2.1. We therefore introduced a parameter to allow for third light in the TESS light curve, $l_{3,\rm TESS}$. Instead of fitting directly for eccentricity, e, and the argument of periastron, ω, we use the decorrelated parameters $\sqrt{e}\sin\omega$ and $\sqrt{e}\cos\omega$, which perform better at low eccentricities (Ford 2006). Our model also includes the radial-velocity semi-amplitude of the host star, K_*, and the system velocity, γ.

To account for different zero-points between HARPS and FEROS we also include a radial-velocity offset for the FEROS data with respect to HARPS, $\Delta\gamma_{\rm FEROS}$. To allow for astrophysical and/or instrumental noise not included in the formal radial-velocity uncertainties we add a radial-velocity jitter term in quadrature to the formal radial-velocity uncertainties. To obtain a spectroscopic reduced χ^2 of unity, jitter terms of 5.5 m s^{-1} for HARPS and 19.0 m s^{-1} for FEROS are required. These jitter terms are in line with expectations for these instruments and a star of this brightness (e.g., Raynard et al. 2018; Hartman et al. 2019, 2020). The bisector span shows no significant correlation with radial velocity.

We used EMCEE (Foreman-Mackey et al. 2013) to explore the parameter space around each candidate orbital period using the likelihood function $\mathcal{L}(d|m) = \exp(-\chi^2/2)$. We initiated 36 Markov chains and generated 100,000 trial steps. We discarded the first 50,000 as burn-in and visually confirmed the sampler had converged. Median parameter values for the best-fitting model at $P_{11} = 35.46$ days are reported in Table 1, and the uncertainties are estimated using the 16$^{\rm th}$ and 84$^{\rm th}$ percentiles of the cumulative posterior distributions.

Figure 2 shows how the best-fitting χ^2 depends on the orbital period alias. Our best fit is to $P_{11} = 35.46$ days, and the next best-fitting candidate period (P_{12}) has $\Delta\chi^2 = 11.3$, which makes it more than 250 times less probable. It is important to understand that the fits to the different period aliases in Figure 2 are effectively a single fit (with identical model and free parameters) exploring a complex χ^2 space with multiple widely spaced minima (at the periods allowed by the photometry in Section 2.3). The $\Delta\chi^2$ plotted is identical to ΔBIC (Bayesian information criterion).

Our best-fitting model is shown in Figure 1, and the corresponding parameters are listed in Table 1. This shows NGTS-11 b to be an exoplanet with a mass and radius very similar to those of Saturn (see Figure 3).

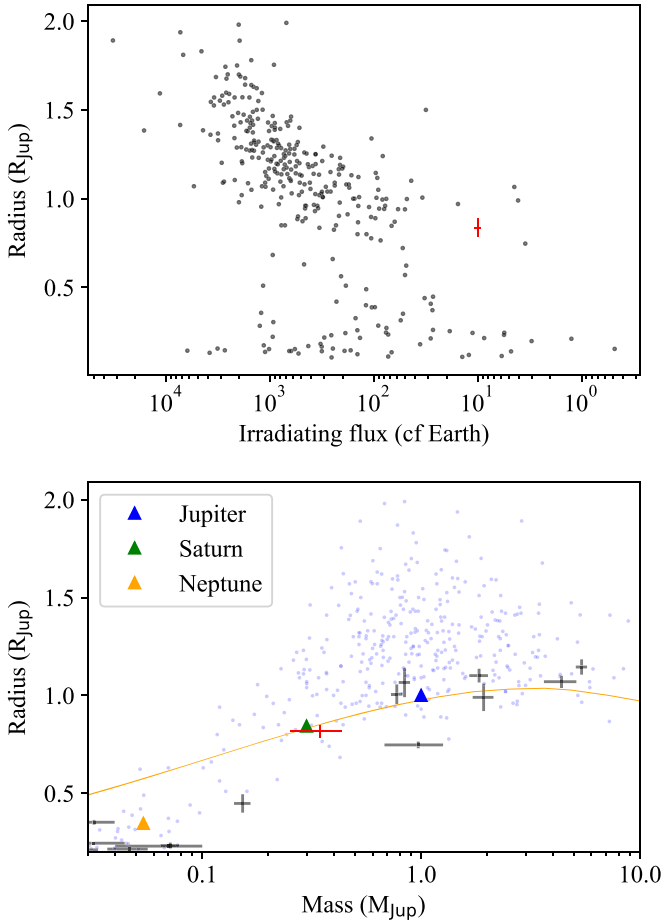

Figure 3. Upper panel: radius-irradiation diagram of well-characterized transiting exoplanets (mass to better than 50% precision and radius to better than 20%; https://exoplanetarchive.ipac.caltech.edu/, accessed 2020 April 30). NGTS-11 b is indicated in red. Lower panel: mass–radius diagram for giant exoplanets from the same sample. Planets with orbital periods longer than 30 days are plotted in black, and those with periods shorter than 30 days in blue. NGTS-11 b is again represented with a red star and solar system giants are indicated with triangles. The orange line shows a theoretical mass–radius relation for a cold hydrogen/helium exoplanet (Seager et al. 2007).

3. Discussion and Conclusions

Following-up a single-transit event identified in our TESS light curve of the K-dwarf NGTS-11, we have detected a second transit event with NGTS. Combined with radial-velocity follow-up with CORALIE, HARPS, and FEROS, these transit detections show that the companion object is an exoplanet with a mass and radius similar to those of Saturn. The planet has a 35.46 day orbit that is marginally eccentric. NGTS-11 b is the first exoplanet to be confirmed after initially being identified as a TESS single-transit event. At our request, NGTS-11 b has also been designated TOI-1847b.

Figure 3 puts NGTS-11 b into context with the wider population of well-characterized exoplanets. The planet radius is not inflated compared to the solar system giants, as expected for a wide-separation planet (Laughlin et al. 2011; Sestovic et al. 2018; Thorngren & Fortney 2018), and its composition is consistent with that of Saturn. NGTS-11 b has a surface gravity, g_p, of $14.1\pm^{5.3}_{3.4}$ m s^{-2}, calculated using the method of Southworth et al. (2007). Assuming an albedo similar to Saturn (0.342; Hanel et al. 1983), we calculate an equilibrium temperature of only $435\pm^{34}_{32}$ K. Since the host star is a K-dwarf, this equilibrium temperature is lower even than some longer-period planets with F- and G-type hosts. In fact NGTS-11 b is one of just a handful of transiting gas giant planets with an equilibrium temperature <500 K. This makes NGTS-11 b an interesting prospect for transmission spectroscopy to study an atmosphere that is much cooler than the typically studied hot Jupiters, which have equilibrium temperatures of 1000–2500 K (e.g., Sing et al. 2016). Assuming a Saturn-like atmospheric composition (2.07 g mole^{-1})[22] we estimate an atmospheric scale height, H_p, of $141\pm^{74}_{51}$ km, which may make it a viable target for transmission spectroscopy. The long baseline between the two transit detections already provides good precision for predicting future transits. For instance, the uncertainty in the timing of transit events in 2025 is only 28 minutes.

It is important to note that we have been able to determine the mass and radius of this relatively long-period exoplanet with a very modest number of radial-velocity measurements (nine with HARPS and six with FEROS). The detection of the second transit with NGTS was crucial for tightly constraining the possible orbital periods, and this serves to demonstrate the value of intense photometric monitoring in following-up single-transit events. Without this second transit detection we would have required many more radial-velocity measurements in order to confirm the planet, determine its orbital period, and measure its mass (e.g., Díaz et al. 2020). The strategy of large investments of photometric follow-up with instruments such as NGTS thereby allows efficient confirmation of single-transit events without adding to the considerable pressure on high-precision radial-velocity instruments. This highlights the power of high-precision ground-based photometric facilities in revealing longer-period transiting exoplanets that TESS alone cannot discover.

The NGTS facility is operated by the consortium institutes with support from the UK Science and Technology Facilities Council (STFC) under projects ST/M001962/1 and ST/S002642/1.

This paper includes data collected with the TESS mission, obtained from the MAST data archive at the Space Telescope Science Institute (STScI). Funding for the TESS mission is provided by the NASA Explorer Program. STScI is operated by the Association of Universities for Research in Astronomy, Inc., under NASA contract NAS 526555.

This work is based on observations made with ESO Telescopes at the La Silla Paranal Observatory under program IDs 0104.C − 0413 (PI RB), 0104.C − 0588 (PI FB), Opticon:2019A/037 (PI DB), and CNTAC: 0104.A − 9012 (PI JIV).

The contributions at the University of Warwick by P.J.W., R.G.W., D.L.P., D.J.A., D.R.A., S.G., and T.L. have been supported by STFC through consolidated grants ST/L000733/1 and ST/P000495/1. D.J.A. acknowledges support from the STFC via an Ernest Rutherford Fellowship (ST/R00384X/1). Contributions at the University of Geneva by F.B., L.N., M.L., O.T., and S.U. were carried out within the framework of the National Centre for Competence in Research "PlanetS" supported by the Swiss National Science Foundation (SNSF). The contributions at the University of Leicester by M.R.G. and M.R.B. have been supported by S.T.F.C. through consolidated grant ST/N000757/1. S.L.C. acknowledges support from the STFC via an Ernest Rutherford Fellowship (ST/R003726/1).

[22] https://nssdc.gsfc.nasa.gov

This project has received funding from the European Union's Horizon 2020 research and innovation program under grant agreement No 730890. A.J., R.B., and M.H. acknowledge support from project IC120009 "Millennium Institute of Astrophysics (MAS)" of the Millennium Science Initiative, Chilean Ministry of Economy. A.J. acknowledges additional support from FONDECYT project 1171208. R.B. acknowledges support from FONDECYT Post-doctoral Fellowship Project 3180246. J.S.J. is supported by funding from Fondecyt through grant 1161218 and partial support from CATA-Basal (PB06, Conicyt). M.N.G. acknowledges support from the Juan Carlos Torres Fellowship. A.Ch. acknowledges the support of the DFG priority program SPP 1992 "Exploring the Diversity of Extrasolar Planets" (RA 714/13-1). J.I.V. acknowledges support from CONICYT-PFCHA/Doctorado Nacional-21191829. E.G. gratefully acknowledges support from the David and Claudia Harding Foundation in the form of a Winton Exoplanet Fellowship. T.H. acknowledges support from the European Research Council under the Horizon 2020 Framework Program via the ERC Advanced Grant Origins 83 24 28. This research has made use of NASA's Astrophysics Data System Bibliographic Services and the SIMBAD database, operated at CDS, Strasbourg, France. This research made use of Astropy,[23] a community-developed core Python package for Astronomy (The Astropy Collaboration et al. 2018).

ORCID iDs

Samuel Gill https://orcid.org/0000-0002-4259-0155
Peter J. Wheatley https://orcid.org/0000-0003-1452-2240
Benjamin F. Cooke https://orcid.org/0000-0002-8824-9956
Andrés Jordán https://orcid.org/0000-0002-5389-3944
Louise D. Nielsen https://orcid.org/0000-0002-5254-2499
Daniel Bayliss https://orcid.org/0000-0001-6023-1335
David R. Anderson https://orcid.org/0000-0001-7416-7522
Jose I. Vines https://orcid.org/0000-0002-1896-2377
Monika Lendl https://orcid.org/0000-0001-9699-1459
David J. Armstrong https://orcid.org/0000-0002-5080-4117
Rafael Brahm https://orcid.org/0000-0002-9158-7315
Matthew R. Burleigh https://orcid.org/0000-0003-0684-7803
Sarah L. Casewell https://orcid.org/0000-0003-2478-0120
Néstor Espinoza https://orcid.org/0000-0001-9513-1449
Edward Gillen https://orcid.org/0000-0003-2851-3070
Nolan Grieves https://orcid.org/0000-0001-8105-0373
Maximilian N. Günther https://orcid.org/0000-0002-3164-9086
Thomas Henning https://orcid.org/0000-0002-1493-300X
Melissa J. Hobson https://orcid.org/0000-0002-5945-7975
James S. Jenkins https://orcid.org/0000-0003-2733-8725
Hugh P. Osborn https://orcid.org/0000-0002-4047-4724
Don Pollacco https://orcid.org/0000-0001-9850-9697
Didier Queloz https://orcid.org/0000-0002-3012-0316
Paula Sarkis https://orcid.org/0000-0001-8128-3126
Alexis M. S. Smith https://orcid.org/0000-0002-2386-4341
Stéphane Udry https://orcid.org/0000-0001-7576-6236
Richard G. West https://orcid.org/0000-0001-6604-5533

[23] http://www.astropy.org

References

Alibert, Y., Carron, F., Fortier, A., et al. 2013, A&A, 558, A109
Asplund, M., Grevesse, N., Sauval, A. J., & Scott, P. 2009, ARA&A, 47, 481
Bakos, G., Noyes, R. W., Kovács, G., et al. 2004, PASP, 116, 266
Blanco-Cuaresma, S., Soubiran, C., Heiter, U., & Jofré, P. 2014, A&A, 569, A111
Borucki, W. J., Koch, D., Basri, G., et al. 2010, Sci, 327, 977
Brahm, R., Jordán, A., & Espinoza, N. 2017, PASP, 129, 034002
Bryant, E. M., Bayliss, D., McCormac, J., et al. 2020, MNRAS, 494, 5872
Choi, J., Dotter, A., Conroy, C., et al. 2016, ApJ, 823, 102
Cooke, B. F., Pollacco, D., West, R., McCormac, J., & Wheatley, P. J. 2018, A&A, 619, A175
Dalba, P. A., Gupta, A. F., Rodriguez, J. E., et al. 2020, AJ, 159, 241
Díaz, M. R., Jenkins, J. S., Feng, F., et al. 2020, MNRAS, in press
Dotter, A. 2016, ApJS, 222, 8
Doyle, A. P. 2015, PhD thesis, Keele Univ.
Eisner, N. L., Barragán, O., Aigrain, S., et al. 2020, MNRAS, 494, 750
Ford, E. B. 2006, ApJ, 642, 505
Foreman-Mackey, D., Hogg, D. W., Lang, D., & Goodman, J. 2013, PASP, 125, 306
Fortney, J. J., Marley, M. S., & Barnes, J. W. 2007, ApJ, 659, 1661
Gaia Collaboration, Brown, A. G. A., Vallenari, A., et al. 2018, A&A, 616, A1
Gill, S., Bayliss, D., Cooke, B. F., et al. 2020a, MNRAS, 491, 1548
Gill, S., Cooke, B. F., Bayliss, D., et al. 2020b, MNRAS, 495, 2713
Gillon, M., Triaud, A. H. M. J., Demory, B.-O., et al. 2017, Natur, 542, 456
Gray, R. O. 1999, SPECTRUM: A Stellar Spectral Synthesis Program v2.76, Astrophysics Source Code Library, ascl:9910.002
Gustafsson, B., Edvardsson, B., Eriksson, K., et al. 2008, A&A, 486, 951
Hanel, R. A., Conrath, B. J., Kunde, V. G., Pearl, J. C., & Pirraglia, J. A. 1983, Icar, 53, 262
Hartman, J. D., Bakos, G. Á., Bayliss, D., et al. 2019, AJ, 157, 55
Hartman, J. D., Jordán, A., Bayliss, D., et al. 2020, AJ, 159, 173
Jones, H. R. A., Butler, R. P., Tinney, C. G., et al. 2004, in ASP Conf. Ser. 321, Extrasolar Planets: Today and Tomorrow, ed. J.-P. Beaulieu, A. Lecavelier des Etangs, & C. Terquem (San Francisco, CA: ASP), 298
Kasting, J. F., Whitmire, D. P., & Reynolds, R. T. 1993, Icar, 101, 108
Kaufer, A., Stahl, O., Tubbesing, S., et al. 1999, Msngr, 95, 8
Kopparapu, R. K., Ramirez, R., Kasting, J. F., et al. 2013, ApJ, 765, 131
Laughlin, G., Crismani, M., & Adams, F. C. 2011, ApJL, 729, L7
Lendl, M., Bouchy, F., Gill, S., et al. 2020, MNRAS, 492, 1761
Maxted, P. F. L. 2018, A&A, 616, A39
Nottale, L., Ceccolini, D., da Rocha, D., et al. 2004, in ASP Conf. Ser. 321, Extrasolar Planets: Today and Tomorrow, ed. J.-P. Beaulieu, A. Lecavelier des Etangs, & C. Terquem (San Francisco, CA: ASP), 355
Oelkers, R. J., & Stassun, K. G. 2018, AJ, 156, 132
Osborn, H. P., Armstrong, D. J., Brown, D. J. A., et al. 2016, MNRAS, 457, 2273
Pepe, F., Mayor, M., Rupprecht, G., et al. 2002, Msngr, 110, 9
Pollacco, D. L., Skillen, I., Collier Cameron, A., et al. 2006, PASP, 118, 1407
Queloz, D., Henry, G. W., Sivan, J. P., et al. 2001, A&A, 379, 279
Raynard, L., Goad, M. R., Gillen, E., et al. 2018, MNRAS, 481, 4960
Ricker, G. R., Winn, J. N., Vanderspek, R., et al. 2015, JATIS, 1, 014003
Sandford, E., Espinoza, N., Brahm, R., & Jordán, A. 2019, MNRAS, 489, 3149
Seager, S., Kuchner, M., Hier-Majumder, C. A., & Militzer, B. 2007, ApJ, 669, 1279
Seager, S., & Mallén-Ornelas, G. 2003, ApJ, 585, 1038
Sestovic, M., Demory, B.-O., & Queloz, D. 2018, A&A, 616, A76
Sing, D. K., Fortney, J. J., Nikolov, N., et al. 2016, Natur, 529, 59
Southworth, J., Wheatley, P. J., & Sams, G. 2007, MNRAS, 379, L11
The Astropy Collaboration, Price-Whelan, A. M., Sipőcz, B. M., et al. 2018, AJ, 156, 123
Thorngren, D. P., & Fortney, J. J. 2018, AJ, 155, 214
Villanueva, S., Jr., Dragomir, D., & Gaudi, B. S. 2019, AJ, 157, 84
Wheatley, P. J., West, R. G., Goad, M. R., et al. 2018, MNRAS, 475, 4476
Yao, X., Pepper, J., Gaudi, B. S., et al. 2019, AJ, 157, 37
Yee, J. C., & Gaudi, B. S. 2008, ApJ, 688, 616